BIMScript: Material-Aware Structured Scene Programs for BIM Ingestion

Prakash Naikade[1,2,3], Thomas Moeslund[1,2,3], and Andreas Møgelmose[1,2,3]

[1] AI:Xpertise Lab, Aalborg University, Denmark
[2] Visual Analysis and Perception Laboratory, Aalborg University, Denmark
[3] Pioneer Centre for Artificial Intelligence, Denmark

https://BIMScriptWorld.github.io/BIMScript/

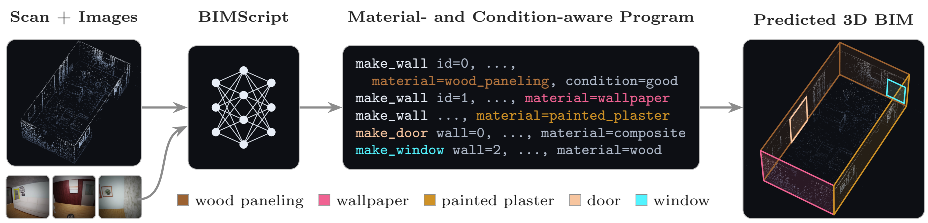

Fig. 1: BIMScript turns a scan into a material- and condition-aware BIM program. A point cloud and its egocentric keyframes are encoded jointly; the decoder emits a structured program in which every element carries geometry, material, and condition, and each command maps one-to-one onto a native Revit/IFC object.

Abstract. Structured-language models such as SceneScript reconstruct a scene as a short program of parametric commands, an inherently editable and semantically explicit representation. We ask three questions that stand between such models and their most compelling application, automated ingestion of existing buildings into BIM tools, studied here on synthetic scans: *what* is the scene made of, *how fast* can it be produced, and *exactly where* is each element. BIMScript answers all three within one grammar. First, we extend the layout language with per-element *material* and *condition* attributes, supervised by a vision-language-model material-passport corpus we build over 100k synthetic scenes (1.9M pseudo-labeled elements), and route image appearance to the material tokens through a lifted-feature point encoder. Second, we show that autoregressive decoding of these programs is dominated not by compute but by kernel-launch and host-synchronization overhead, and remove it with an output-exact CUDA-graph decoder (1.9 vs 6.4 ms/step, 3.4×) plus a grammar-parallel, tolerance-verified draft-and-verify scheme that exploits the deterministic entity schema. Third, we address the model's 5cm token-grid granularity with training-free geometric snapping and a hybrid discrete–continuous decoder head that regresses a sub-bin offset, and measure how much of the residual error each recovers. Because each command maps one-to-one onto a native Revit object, we validate direct ingestion into a BIM authoring tool end to end with a working add-in and its IFC4 export, and the same program's language form is designed to support LLM-driven, sustainability-aware reasoning over the built asset.

Keywords: 3D scene understanding · Structured language models · Efficient decoding · Material recognition · Building Information Modeling

1 Introduction

The built environment is responsible for a large share of global material consumption and carbon emissions, and the overwhelming majority of the buildings that will exist in 2050 already stand today [41, 50]. Decarbonizing, renovating, re-valuing, or eventually disassembling these assets increasingly relies on a digital model of *what is already there* [9, 14]. In practice such models are Building Information Models (BIM): parametric, object-level descriptions of walls, openings, slabs, floors and their properties, consumed by tools such as Autodesk Revit and exchanged through open standards like IFC [25]. Producing a BIM of an existing building, however, remains a slow, largely manual "scan-to-BIM" process [34, 49, 54]: a surveyor captures a point cloud, and a modeler hand-traces geometry and hand-labels properties element by element.

Structured-language models offer an appealing shortcut. SceneScript [5] reconstructs a scene not as a mesh or an occupancy grid but as a short *program*, a sequence of parametric commands such as `make_wall` and `make_door`, emitted autoregressively by a transformer decoder conditioned on an encoded point cloud. The representation is compact, human-readable, directly editable, and, crucially, already shaped like the object model a BIM authoring tool expects. Yet three gaps separate this elegant formulation from practical as-built BIM ingestion, and they map onto *three questions*: (1) *What is in the scene*? SceneScript predicts geometry and coarse class, but a BIM element is defined as much by its *material* and *condition* as by its shape. A wall is not merely a wall: it is a *brick* wall in *good* condition, and that attribute drives every downstream sustainability workflow. The layout grammar carries no such information. (2) *Fast*? Autoregressive decoding of one scene program takes on the order of seconds on a modern GPU. For interactive modeling and for ingesting building stock at portfolio scale, this is the binding constraint. (3) *Exactly where*? SceneScript itself notes that high-level commands "can be challenging to capture fine-grained geometric details with extremely high precision (i.e. mm)". In the reference configuration this is not a vague limitation but an exact one: coordinates are discretized onto a 5cm grid, so nearest-bin quantization alone has a worst-case error of ± 2.5 cm before any model error, below the tolerance BIM level-of-accuracy (LOA) and level-of-development (LOD) specifications demand [2, 39, 52].

BIMScript answers all three questions within a single, backward-compatible grammar, and is designed around the payoff: each command corresponds one-to-one with a native Revit/IFC object (Sec. 8), so the emitted program is positioned to ingest directly into BIM authoring tools; and because the scene is expressed in language, it becomes a first-class input to large language models (LLMs) for downstream, sustainability-aware Architecture, Engineering, and Construction (AEC) reasoning: real-estate valuation, life-cycle assessment (LCA), adaptive-reuse and disassembly planning, and circular-economy waste reduction.

Our key contributions are:

- *What*: We propose BIMScript, a material- and condition-aware scene language, and build a material-passport corpus of 1,900,908 pseudo-labeled elements over ≈100k scenes to supervise it; a lifted-feature point encoder routes image appearance to the material tokens.
- *Fast*: We profile decoding, show that ∼65% of it is kernel-launch and host-synchronization overhead rather than compute, and remove that overhead with an output-exact CUDA-graph decoder (3.4×), with a grammar-parallel, tolerance-verified draft-and-verify scheme that exploits the deterministic entity schema.
- *Exactly where*: We add training-free geometric snapping and a hybrid head that regresses a bounded within-bin offset, with the 5cm grid's contribution to coordinate error measured directly.
- Lastly, we publish a public-artifact reproduction audit of SceneScript, and a working BIMScript-to-Revit adapter that creates native elements carrying material and condition parameters.

2 Related Work

2.1 Floorplan reconstruction and scan-to-BIM.

A long line of work reconstructs floorplans and layouts from scans, e.g. FloorNet [29], MonteFloor [46], RoomFormer [59], PolyRoom [31], FRI-Net [57] and CAGE [30], or aligns CAD models to RGB-D scans [4]; large scan and layout datasets underpin them [1, 3, 5, 8, 13, 15, 18, 60]. In the AEC community, scan-to-BIM is typically a multi-stage geometric-fitting pipeline [34, 49, 54]. These methods target geometry and topology; material and condition are added manually afterwards. BIMScript predicts geometry, material, and condition jointly in one autoregressive pass and emits a program that is already an object model.

2.2 Structured-language scene models.

SceneScript [5] recasts layout estimation as next-token prediction over a domain-specific command language, following a broader line of work that treats geometry as language: PolyGen for meshes [36], DeepCAD [55] and CAD-as-Language [17] for parametric CAD. These inherit the transformer decoder [53] and its autoregressive cost. Fast SceneScript (FSS) [58] accelerates SceneScript with multi-token prediction (MTP) and self-speculative decoding, reducing iteration count at a small quality cost. BIMScript differs on all three axes: we add *semantics* (materials) rather than only geometry, we attack decode *overhead* before iteration count (an orthogonal and multiplicative gain), and we replace generic MTP with a *grammar-parallel* scheme that is exact by construction because the entity schema makes future token *types* deterministic. Xie *et al*. [56] also bring NLP-style *infilling* to SceneScript, but for a different problem and by a different mechanism: their human-in-the-loop local correction rearranges the sequence FIM-style and regenerates the masked entities *token by token*, trained from scratch with pose anchoring. Our `[INFILL]` embedding instead masks slots *in place* and uses the schema-determined slot types to draft a whole entity in a *single* verified forward pass. For them infilling is the task; for us it is an acceleration primitive added to an existing checkpoint by a short fine-tune.

2.3 Efficient autoregressive decoding.

Speculative decoding [11, 28], multi-token prediction [10, 20], blockwise parallel decoding [47], KV-caching and multi-query attention [43], and CUDA graphs [21] all reduce transformer inference cost. Most target large language models where each step is compute-heavy. SceneScript's decoder is tiny (a step through 4 layers of width $d = 512$ is $\sim$2 MFLOPs), so the dominant cost is overhead, which reframes which of these tools matter, as we show in Sec. 5.

2.4 Material passports, BIM, digital twins, and circular economy.

Material recognition from images is well studied [6, 7, 42, 51], but almost always as 2D image labeling. Connecting per-pixel or per-region material evidence to *3D building elements* in a reconstruction, at scale and without per-scene manual annotation, is the gap BIMScript's material-passport pipeline fills, using a vision-language model [19] to distill appearance into element-level labels.

Material passports [24, 33] and circularity indicators [23, 40] require element-level material inventories; BIM-based LCA [45] requires geometry and materials in a machine-readable model. BIMScript (Fig. 2) produces exactly this inventory automatically. A broader survey of XR/AI for AEC situates this direction [35].

3 Background and a Reproducible Baseline

3.1 SceneScript in brief

SceneScript encodes a point cloud with a sparse-convolutional encoder [12, 48] and decodes a command program with a transformer decoder attending to the encoded context. Continuous parameters (coordinates, sizes) are discretized into B bins over a fixed world range and predicted as categorical tokens; a small type finite-state machine (FSM) constrains which token kind is legal at each step. In the configuration matching the public checkpoint the world range is $[0, 32]$ m and B=640, giving a $32/640$ = 5cm grid, the paper's stated point cloud resolution.

3.2 Compatibility and target-coverage issues

Naive training does not reproduce the public checkpoint's behavior, for two reasons worth recording for any follow-up work on this family. First, a *discretization/reconstruction mismatch*: the tokenizer pairs a rounding rule at discretization with a reconstruction rule at decode, and pairing floor-rounding with bin-edge reconstruction biases every coordinate by up to a full bin, which alone

Table 1: Reproducing the SceneScript point-only encoder–decoder from public artifacts for layout estimation. *Top*: 1,000 held-out test scenes, same evaluator, one greedy decode per model, so F1@5cm and both AvgF1 columns come from a single set of predictions. "Local-FSS" is our reimplementation of Fast SceneScript's 20-threshold average (Sec. 3.3); parameters are measured from the instantiated models. *Bottom*: numbers as published, on each paper's own split and evaluator, neither of them public.

Model	Params (M) ↓			F1@5cm ↑	AvgF1 ↑	AvgF1 (local-FSS) ↑
	Enc.	Dec.	Total			
Public ckpt	10.47	15.38	25.85	0.581	0.667	0.931
Ours (640-bin grid)	20.15	36.42	56.57	0.554	0.658	0.930
Ours (2048-bin grid)	20.15	37.86	58.01	0.570	0.672	0.896
SceneScript Table 2	≈ 20	≈ 35	≈ 55	0.848	0.784	–
FSS Table 1 (SSD, n=10)	–	15.05	–	–	–	0.912

pushes wall-corner error past the F1@5cm threshold irrespective of model quality. Second, a *translation-frame* issue: anchoring the coordinate frame at the observed point-cloud minimum places ground-truth geometry of *unobserved* floor area at negative coordinates, which the tokenizer then discards, a silent recall loss of 46,218 removal events in one training run (Sec. C). We adopt the unbiased pairing (round at discretize, edge at reconstruct) and a margin-anchored frame with a bounded clamp, applied identically at train and inference.

Section C gives both derivations, the controlled A/B that identifies which convention is consistent with the released weights, the measured round-trip oracle, and the mitigation's residual cost (0.6% of entities at evaluation time), rather than asserting either issue is fully resolved.

3.3 Reproduction parity, and what the token grid buys

What public artifacts can support. SceneScript's published Table 2 (mean F1@5cm 0.848) cannot be audited from public artifacts. The released checkpoint's value-embedding matrix has 646=640+6 rows and 2,000 learned positions, whereas the paper states a vocabulary of 2,048, so the released artifact does not match the paper-described architecture; the dataset splits are not public; and Fast SceneScript, which retrains the same architecture, reports no F1@5cm at all. Concretely, the released weights score 0.581 mean F1@5cm on our test split against the paper's 0.848 on its own (non-public) split; we cannot attribute that difference, so we treat the artifact, not the published table, as the reproduction target. The released checkpoint is therefore the only verifiable anchor, and we anchor every claim to it on fixed splits of our own. Two controls then separate evaluator validity from training validity. For the *evaluator*, our reimplementation of an FSS-style threshold protocol scores the released checkpoint 0.931 AvgF1, against the 0.896 Fast SceneScript reports for the same weights on their different split. For *training*, on identical scenes with a single decode per scene, our retrained model reaches 0.930 local-FSS AvgF1 against the released checkpoint's 0.931 (Tab. 1). We read this as evidence that our training path reaches the released artifact's behavior, not as a general equivalence claim. Our runs carry 2.19× (640-bin) and 2.24× (2,048-bin) the released checkpoint's parameters, but both sit within 3% of the ≈55M SceneScript specifies, so the gap is the released artifact being roughly half the size of its own paper's architecture rather than our models being oversized. The same predictions yield 0.667 under our dense-threshold protocol and 0.931 under the local FSS-style one, so "mean F1" is protocol-dependent: we report both and never compare across them.

The token grid is a modest, two-sided knob. A 300-scene round-trip through our tokenizer (Sec. C) shows the representation is not the binding cap: ground truth reconstructed through the tokenizer scores 0.994 F1@5cm at 640 bins, and frame-boundary censoring removes only 0.6% of entities. The residual error is instead *amplified* by grid pitch, since on a 640-bin (5cm) grid a ±1-bin error is already a 5–10 cm miss while on a 2,048-bin (1.56 cm) grid the same error passes. We therefore decouple the *language* grid from the point-cloud voxel grid, leaving the input at 640 bins while the value vocabulary becomes an independent knob, and train a matched-budget 2,048-bin run. The effect is real but small and cuts both ways: strict F1@5cm rises 0.554 → 0.570 while the coarse local-FSS average falls 0.930 → 0.896 (Tab. 1). A finer grid therefore buys strict-threshold precision and gives back some coarse-threshold robustness. We report it as a design trade-off rather than as the explanation for the distance to the published number, and keep both grids in play in what follows. Training curves and a recipe negative result are in Sec. C.

4 BIMScript: What Is in the Scene

4.1 Material-aware scene language

We keep SceneScript's flat, definition-driven grammar and extend the parameter list of each building element with two inline categorical attributes:

```
make_wall,  id=0, a_x=.., .., b_z=.., height=..,
            thickness=0.0, material=painted_plaster, condition=good
make_door,  id=1000, wall0_id=0, position_x=.., .., width=..,
            height=.., material=composite, condition=new
make_window,id=2000, wall0_id=0, position_x=.., .., width=..,
            height=.., material=aluminum, condition=good
```

Inline attributes ride the existing categorical value-token space (the class index lives below the numeric-bin range, so the vocabulary does not grow), require no decoder change, and, decisively, condition each material token on the element's *own* geometry tokens through self-attention. We deliberately avoid a separate `set_material,target_id=..` command block: decoded element ids are positional and regenerated at decode time, so cross-referencing a separately predicted attribute to its element is brittle, and it roughly doubles sequence length. Materials use atomic `snake_case` labels from a closed taxonomy; the two attributes add ∼2 tokens per element (∼40 per scene), comfortably within the 2048-token budget. The taxonomies are frozen and append-only, so the type-token enumeration

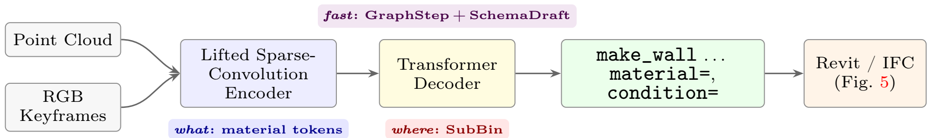

Fig. 2: BIMScript overview. A lifted-feature encoder routes image appearance into the point encoder, so the decoder can condition each material and condition token on the element's own geometry tokens. Decoding is accelerated by *GraphStep* and *SchemaDraft* and refined below the token grid by *SubBin* (Fig. 4), and every emitted command maps one-to-one onto a native Revit/IFC object.

extends the layout enumeration without renumbering: every layout checkpoint stays valid and material models warm-start from one.

4.2 A material-passport corpus at scale

Aria Synthetic Environment (ASE) [5,16] dataset's synthetic indoor scenes give exact ground-truth *geometry* but no per-element material labels. We generate them with a per-scene *material passport*: for every element we gather the RGB observations that project onto it and prompt a vision-language model [19] on the resulting crops for a material and condition label. Two further cues, a dense material-segmentation predictor and classical color/texture statistics, are computed independently and stored beside it. They do not supply the label; they measure how far it can be trusted (Sec. A). Geometry lines are copied verbatim from ground truth, so layout supervision is byte-identical to the layout task.

The corpus (Tab. 6) has 99,990 scenes and 1,900,908 elements over a 14-material, 5-condition taxonomy, with zero join failures. The full material and condition taxonomies are [`aluminum`, `brick`, `composite`, `concrete`, `glass`, `metal`, `painted_plaster`, `pvc`, `stone`, `tile`, `wallpaper`, `wood`, `wood_paneling`, `unknown`] and [`new`, `good`, `worn`, `damaged`, `unknown`], respectively. Two properties matter for honest evaluation. The distribution is heavily imbalanced (`good` covers 83% of conditions, `damaged` just 0.05%), so we report macro-F1 alongside accuracy. And the pseudo-labels are noisy: the VLM agrees with the classical-CV cue on only ∼25% of elements and with the dense-segmentation cue on ∼34%. That low agreement is evidence that materials are genuinely hard to pin down from any single cue, so some of the residual error in Tab. 3 belongs to the labels rather than to BIMScript. It is not a formal bound on achievable accuracy.

4.3 Getting appearance to the material tokens

Materials are an *appearance* property, but SceneScript's geometric point encoder discards color. The design question is whether appearance survives the path from pixels to the material token. We route it through a *lifted-feature* encoder: a frozen 2D backbone extracts a dense feature map per keyframe; features are projected to per-3D-point vectors by pose projection, aggregated across observing keyframes,

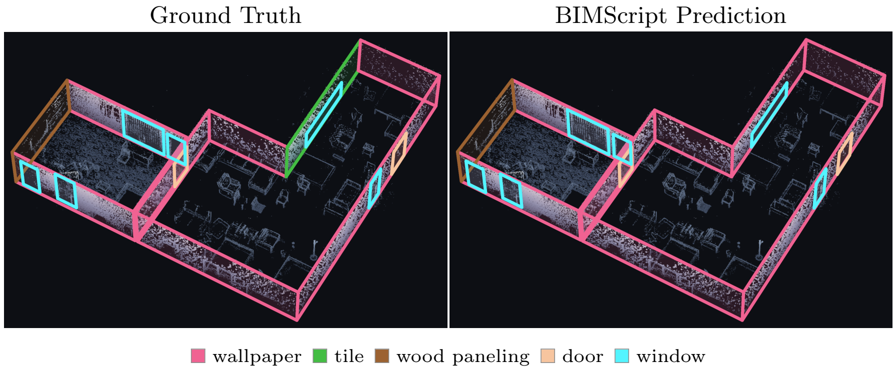

Fig. 3: A decoded BIMScript program over the input point cloud, wall faces colored by predicted material and openings by role. On this 18-element, three-room validation scene every ground-truth element is recovered (coverage 1.0, F1@5cm 0.944), and 16 of 18 carry the correct material, at 0.944 condition accuracy. The one visible attribute error, the `tile` wall at the rear predicted `wallpaper`, is the frequent-class collapse that Tab. 4 quantifies at corpus scale.

and appended to the point's XYZ as extra input channels to the sparse encoder. The decoder, tokenizer, and grammar are unchanged.

Two implementation details proved essential. *Occlusion filtering:* naive pose projection paints every surface along a ray, and testing projected points against the ground-truth depth removes those wrong-surface features, 46% of correspondences on one measured scene. *Feature source:* deep semantic features (ResNet-50 [22] `layer4`) are spatially coarse, whereas materials live in color and texture, so we ablate shallower layers (`layer2`/`layer3`), DINOv2 [38] and DINOv3 [44] dense features, raw per-point RGB, and RGB-appended variants (Tab. 3). Because re-lifting the full corpus is expensive, the feature source is chosen once on a small subset and then fixed before the corpus is lifted.

5 FastBIMScript: Efficient Decoding

5.1 Where the time actually goes

Decoding one scene on A100 takes 1.4–1.8 s against 0.7–0.8 s for the encoder, so decode is the target. The useful measurement is *per step*, and three observations locate the cost, see Tab. 2. Per-step time is flat from step 20 to 600, so it does not grow with sequence length. The step is nowhere near FLOP-bound: a $d = 512$, 4-layer, single-token step is about 2 MFLOPs, microseconds of A100 compute. And pre-allocated static buffers are no faster than growing ones, so memory reallocation is not the cost either. What remains is *overhead*: roughly 100 tiny kernel launches per step, plus one host synchronization forced by the type FSM reading a GPU tensor back into Python at every step. Collapsing the step into a single CUDA graph removes exactly that, cutting 5.49 to 1.91 ms/step. The

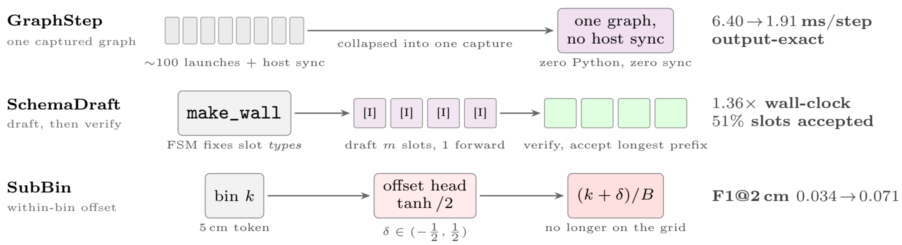

Fig. 4: The three FastBIMScript mechanisms. *GraphStep* collapses a decode step whose cost is kernel-launch and host-synchronization overhead into a single captured CUDA graph, emitting identical tokens. *SchemaDraft* exploits the fact that a command token fixes the *types* of all remaining parameter slots: it drafts them in one forward pass with a learned `[INFILL]` embedding (`[I]`) and accepts the longest verified prefix. *SubBin* keeps the coarse token for structure and adds a bounded within-bin offset, so a coordinate is no longer pinned to the 5cm grid.

Table 2: Decode acceleration, all measured on A100, batch 1, real scenes. *Left*: per-step decode cost; per-step time is flat in sequence length, so the eager→graph gap is overhead, not compute. *Right*: whole-scene wall-clock factors (64 scenes, greedy), smaller than per-step factors because sequence assembly and grammar bookkeeping run outside the graph.

Decode step variant	ms/step ↓	Whole-scene decode	speedup
reference loop (recompute)	6.40	reference (1.31 s/scene)	1.0×
KV cache (growing buffers)	5.43	KV cache	1.31×
KV cache (static buffers)	5.49	+ GraphStep (graph)	1.55×
+ GraphStep (graph)	**1.91**	+ SchemaDraft (τ=2)	1.36×

same reasoning explains why KV-caching alone, the obvious first move, buys only 1.2×: it removes FLOPs from a loop that was never FLOP-bound.

5.2 GraphStep: output-exact CUDA-graph decoding

We compile the entire decode step (embed, self-attention over a static KV buffer, cross-attention over the padded context, feed-forward, final norm, tail projection, argmax, on-device FSM type update, and write-back) into one CUDA graph with zero Python and zero host synchronisation per step; the host syncs only every 16 steps to scan for the `stop` token. The FSM grammar is compiled into device lookup tables whose semantics are proven equal to the reference Python FSM up to the first `stop` token (CPU fuzz test), and the decoded strings are verified equal to the reference decoder on real scenes. The result is *output-exact*, with identical tokens, and needs no retraining. Per-step cost drops 6.40 → 1.91 ms (3.4×); isolating the graph itself from the KV-cache path it builds on, the graph's own contribution is 5.49 → 1.91 ms (2.9×).

5.3 SchemaDraft: grammar-parallel draft-and-verify

Generic multi-token prediction [10, 20], as used by Fast SceneScript, must *guess* how many future tokens to emit and gate them with learned confidence heads. Our grammar removes the guesswork: once a command token is emitted, the FSM fixes the *types* of every remaining parameter slot of that element. We therefore draft all m remaining values in one forward pass, putting a single learned `[INFILL]` embedding in place of each not-yet-known value while position and type embeddings stay intact, then verify them in one teacher-forced pass and accept the longest prefix matching the verifier's argmax: structural slots exactly, numeric slots within a tolerance of τ=2 bins, writing back the verifier's token rather than the draft's. The draft is *schema-complete* rather than learned, so there is no confidence threshold to tune and no extra projection blocks, one embedding row against roughly 7.5% added parameters. At τ=2 the scheme is tolerance-verified rather than output-exact; a strict τ=0 mode would recover exactness, and we report τ=2 because it is the operating point we measured. An element of 11–13 sequential steps becomes about 4 forwards at full acceptance, and this composes with GraphStep.

Acceptance, not drafting, is the binding constraint, because coupled coordinates such as a wall's far corner given its near corner are genuinely ambiguous in a one-shot draft. Whole-element masking during the fine-tune and *intra-element redrafting* at decode time lift acceptance from 38% to 51%; Sec. B gives the mechanism and the evidence that the residual gap is coordinate-coupling ambiguity rather than undertraining. Measured over 64 scenes at τ=2, sequential forwards per scene drop 1.33× and decode wall-clock falls 1.31→0.97 s/scene (1.36× over the reference loop, without GraphStep fusion), while the output agrees with strict greedy decoding on 96.6% of tokens (Tab. 2). The fine-tune itself does not cost geometry (Sec. 7). The same `[INFILL]` capability would serve the human-in-the-loop local-correction task of Xie *et al*. [56] at draft-verify speed.

With decode at 0.85–0.97 s/scene the fp32 sparse encoder (0.7 s) is already co-dominant and bounds what further decode work can return; an fp16 encoder attempt is a negative result reported in Sec. B.

6 Exactly Where: Sub-bin Geometric Refinement

With B=640 bins over $[0, 32]$ m the grid spacing is 5cm, so nearest-bin quantization of a coordinate has a worst-case error of 2.5 cm before any model error is added, below common BIM tolerances [52]. The first step is to make this measurable: we add tight F1 thresholds (0.1–5 cm) as evaluation overrides, never changing the default thresholds that every legacy number depends on. Because the synthetic ground truth is exact, the measurement is clean. We then test two complementary recoveries; the tokens carry topology and semantics, the refinement carries metric precision.

Training-free snapping reads the point cloud directly. For each wall we collect points within a tolerance of the wall rectangle, fit the 2D line by PCA, and re-

Table 3: Appearance-source ablation for material and condition. All six arms share one 2,250-scene training subset, one 20k-step budget, and the same 250 validation scenes, so the comparison isolates the appearance source. Condition macro-F1 is over the three classes every arm's matched population realizes (`good`, `new`, `worn`). Single-seed throughout, so we read the ordering as evidence rather than a settled ranking.

Encoder	Appearance source	Coverage ↑	Material		Condition	
			Accuracy ↑	Macro-F1 ↑	Accuracy ↑	Macro-F1 ↑
point-only	none (geometry)	0.269	0.326	0.259	0.715	0.322
lifted	raw per-point RGB	0.276	0.305	0.220	0.701	0.324
lifted	ResNet-50 `layer2`	0.260	0.347	0.239	0.734	0.337
lifted	ResNet-50 `layer3`	0.259	0.341	0.256	0.729	0.348
lifted	DINOv3 ViT-S/16	0.253	**0.370**	0.245	0.742	0.356
lifted	DINOv2 ViT-S/14	0.267	0.369	**0.257**	**0.769**	**0.366**

project the endpoints onto the fit; doors, windows, and heights follow the same pattern. It is a post-process and sets the bar the learned head must beat.
SubBin keeps the coarse token for structure and adds a small MLP head on the decoder's last hidden state that regresses a within-bin offset per numeric slot, bounded to $(-0.5, 0.5)$ by a $\tanh/2$ activation. Under our round+edge convention the final coordinate is $(\text{bin} + \text{offset})/B$. The head trains with a Huber loss on the pre-rounding residual over numeric slots only, fine-tuned from an existing checkpoint, and its parameters exist only when enabled, so legacy checkpoints load unchanged. At inference one extra teacher-forced pass emits the offsets, composing for free with the SchemaDraft verify pass. Section 7 reports what this recovers, which is real but small, and Sec. B gives the full per-type table.

7 Experiments

Data and protocol. We use the synthetic indoor corpus of Sec. 4.2 with the splits of Tab. 6, and evaluate on the full 1,000-scene validation and test splits. We report layout F1 under both our dense-threshold protocol and a local, FSS-style protocol (Sec. 3.3); material and condition macro-F1 over element pairs matched by the Hungarian algorithm [26] at a 10 cm threshold; and decode latency at batch 1 (single L40S for Tab. 4, single A100 for Tab. 2). All models optimize with AdamW [32] at learning rate 10^{-4} and effective batch 64, following the original recipe. Every number we report is decoded greedily at a fixed decode batch size of 4. Material models fine-tune from a layout checkpoint by type-embedding row surgery, which lets the material grammar reuse a trained layout decoder without renumbering the type enumeration; the *SchemaDraft* and *SubBin* fine-tunes descend from the same reproduction checkpoint.
Adding materials does not cost geometry. The full BIMScript model emits material and condition alongside every geometric parameter, so the first question is what that costs in layout accuracy. On the 1,000-scene test split it scores 0.577 F1@5cm against 0.571 for the point-only layout model on the same grid, splits, and protocol (Tab. 1): the material-aware model is marginally *ahead* of

Table 4: The full BIMScript grammar against its reproduction anchor, on the 1,000-scene *test* split. *Public ckpt* (anchor) emits layout only, so its attribute cells are empty by construction. BIMScript^{+} continues the 40k model for 20k steps with the SchemaDraft and SubBin objectives (Sec. 5, Sec. 6). Layout is scored over all ground-truth elements, attributes only over elements matched within 10 cm (Sec. 7). Latency is batch 1 with the GraphStep decoder on one L40S, the production path; all other metrics come from one greedy decode per scene at batch 4. (*Scene latency tracks emitted program length: the public checkpoint's batch-1 decode emits $\sim 3\times$ more tokens per scene than BIMScript on the same scenes, while per token its 4-layer decoder is about $2\times$ faster than our 8-layer one.)

	F1@5cm ↑				AvgF1 ↑			Material		Condition		Model	
Model	wall	door	window	mean	ours	FSS	Cov. ↑	Acc. ↑	F1 ↑	Acc. ↑	F1 ↑	Par. ↓	s/sc.* ↓
Public ckpt	**0.621**	0.720	0.400	**0.581**	0.667	**0.931**	–	–	–	–	–	**25.9M**	1.47
BIMScript (40k)	0.509	**0.752**	**0.469**	0.577	**0.676**	0.907	**0.701**	0.629	0.285	**0.842**	**0.352**	58.4M	1.14
BIMScript^{+} (60k)	0.513	**0.752**	0.462	0.576	0.669	0.897	0.699	**0.639**	**0.291**	0.840	0.350	58.5M	**1.12**

the layout-only baseline, on a total budget of 40k lifted layout steps plus a 40k-step material fine-tune against the baseline's 200k. The speed and precision fine-tunes are likewise inside the reproduction run's own eval-to-eval noise band (0.56–0.62 F1@5cm). Appearance semantics therefore ride along in the same grammar essentially for free, see Fig. 3.

Appearance decides which attributes are recoverable. Table 3 reports two experiments. The six-arm ablation holds the subset, the budget, and the matched-class population fixed across arms, so it is the experiment that supports an appearance-source ranking. There, material *macro*-F1 is nearly flat, since every arm leans on the taxonomy's frequent classes at this budget, but accuracy and *condition* macro-F1 (over the three classes every matched population realizes) separate the sources: DINOv2 leads condition F1 (0.366 against point-only's 0.322), DINOv3 edges it on material accuracy (0.370 vs 0.369) while trailing on condition (0.356), and raw per-point RGB buys nothing over geometry alone (0.324 against 0.322). A learned, view-stable feature space, not color itself, is what survives lifting and per-point pooling.

Scaling the winning arm to the full corpus (Tab. 4) is what makes the attributes usable: the full-corpus model matches 70% of ground-truth elements and predicts their material at 0.626 accuracy on validation and 0.629 on test.

Condition macro-F1 is the weaker of the two attributes and nearly identical across splits (0.353 val, 0.352 test), improving with the longer fine-tune (0.342 at half the budget). The average is carried almost entirely by `good` (0.914): `new` reaches only 0.144 and `worn`, despite 485 matched test instances, is never recovered. Condition is therefore predicted at the level of "is this the default state or not," and the rare tail (`damaged`, 0.05% of the corpus) is a smaller effect than the failure on `worn`.

Speed. Table 2 gives the decode results, all measured on the same hardware and scenes: *GraphStep* is output-exact, *SchemaDraft* tolerance-verified, and each is reported against the same reference loop. The two compose in principle but not yet in one binary: a draft covers m slots where m varies by command and shrinks during redrafting, so fusing it into GraphStep's capture needs a family of graphs keyed by m rather than a single-token graph. We report the two separately and do not assume the factors multiply.

Precision. The offset head does what the mechanism was designed to do: mean F1@2 cm doubles, $0.034 \rightarrow 0.071$, and door and window MAE fall by 10.3% and 3.2%, while the training-free snapping baseline it is measured against barely moves. Two further measurements then locate where the remaining error actually lives, which is the more useful outcome. Wall MAE stays near 8.7 cm, far above the 1.25 cm quantization alone predicts, so at this operating point wall error is dominated by something other than grid pitch, most plausibly residual mis-association; we have not isolated it. And F1@0.5 cm is zero for every variant. Together these say the 5 cm grid is no longer the binding constraint on precision: sub-centimeter output needs better detection and association, not finer regression. All of this is conditional on an already-correct detection (Tab. 7, Sec. B), the scope the head is designed to operate in.

BIMScript for everything. The speed and precision capabilities above are measured as separate fine-tunes; BIMScript$^+$ folds them into the deployed model, continuing the 40k checkpoint for 20k steps with the `[INFILL]` and sub-bin objectives active. The combined fine-tune is metrically free at the strict threshold (0.576 vs 0.577 test F1@5cm, one decode apart), slightly ahead on material accuracy (0.639 vs 0.629), and slightly behind on the coarse averages (0.669 vs 0.676 AvgF1, 0.897 vs 0.907 local-FSS), at unchanged batch-1 latency (1.12 vs 1.14 s/scene with GraphStep). A single checkpoint therefore serves plain greedy decoding, draft-and-verify, and sub-bin refinement without giving up the metrics of the specialized models (Tab. 4 and Fig. 3).

8 BIM Ingestion and LLM-Driven AEC Reasoning

From program to native BIM. A BIMScript program is already an object model, not merely a geometric description: each command corresponds one-to-one with a native authoring-tool object, and the material and condition attributes attach to that object's own parameters rather than to a side channel. We implement a deterministic BIMScript-to-Revit adapter as a pyRevit [27] add-in and validate it end-to-end. On the tested Revit and exporter version, importing a decoded program creates *native* Revit walls with one wall type per predicted material, hosted door and window family instances, and the material, condition, and source-element id attached as shared parameters on every element (Fig. 5). The same document exports to IFC4 through Revit's own exporter, and the exported file's element classes, hosting relations, and BIMScript property set pass independent validation on the evaluated scenes. Table 5 lists the correspondence between BIMScript commands, Revit API calls, and IFC entities. What this establishes is that native-object ingestion is real, not aspirational; the hard part, getting geometry, material, and condition into one coherent and precise program, is what BIMScript solves.

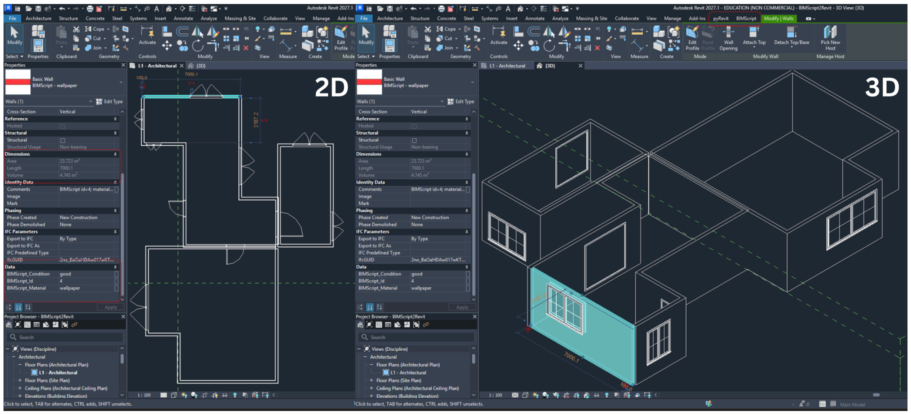

Fig. 5: A decoded BIMScript program ingested into Autodesk Revit by our pyRevit add-in. The imported plan consists of *native* Revit walls, here an instance of the auto-created type *BIMScript - concrete*, and every element carries its predicted material, condition, and source id as shared parameters.

Language as an interface for reasoning. Expressing the scene as language makes it a first-class LLM input [37]. The material- and condition-annotated program is a compact, machine-readable inventory over which an LLM can reason for sustainability-aware AEC tasks: embodied-carbon and life-cycle estimation (BIM-based LCA [45]), material passports and circularity indicators [23,33,40], maintenance triage from the condition attribute (absent from prior structured-scene models), and adaptive-reuse or disassembly decisions.

9 Limitations and Future Work

Our supervision is synthetic and its material labels are VLM-distilled pseudo-labels (Sec. 4.2), so real-scan generalization and label denoising are open. The rare-class tails are thin in both taxonomies (`damaged` at 0.05% of conditions, `glass` at 0.04% of materials), so macro-F1 depends sharply on which classes a matched population happens to realize. Our reproduction claims are audited against public artifacts rather than a verified replication of SceneScript's Table 2 system (Sec. 3.3). GraphStep is batch-1 and argmax by construction, so nucleus sampling and batched decode fall back to the slower path, and SchemaDraft at τ=2 is tolerance-verified rather than output-exact. Draft acceptance plateaus at 51% because of coordinate-coupling ambiguity, so the measured 1.36× sits well short of the 3× full-acceptance bound, and the fused GraphStep×SchemaDraft decoder remains future engineering work. Sub-bin refinement is evaluated on exact synthetic ground truth and conditional on correct detection, which flatters it relative to noisy real scans and end-to-end deployment. The Revit and IFC path is validated on programs decoded from synthetic scenes (Sec. 8), not yet against professional as-built modeling on real scans. The grammar itself is the

Table 5: BIMScript-to-BIM mapping. Both Revit add-in (Fig. 5), and the IFC exporter through Revit's own IFC4 exporter, whose output we validate independently for element classes, hosting relations, and the BIMScript property set on the evaluated scenes.

BIMScript	Revit API target	IFC entity / property set
`make_wall`	`Wall.Create` (curve, level, height)	`IfcWall`
`make_door`	hosted `FamilyInstance` on host wall	`IfcDoor` + `IfcRelFillsElement`
`make_window`	hosted `FamilyInstance` on host wall	`IfcWindow` + `IfcRelFillsElement`
`material=...`	wall/family-type material parameter	`IfcMaterial` / `IfcMaterialLayerSet`
`condition=...`	shared parameter (custom)	custom Pset (*e.g.* `Pset_Condition`)

natural thing to grow next: extending it beyond interiors to facades, structural elements such as beams and columns, and mechanical, electrical, and plumbing (MEP) runs would cover what an as-built model actually has to carry, and would need either real scans or synthetic data close enough to stand in for them. Finally, the LLM-driven reasoning we motivate in Sec. 8 remains future work.

10 Conclusion

We introduced BIMScript, a structured scene language in which every element carries not only geometry but the material and condition that define a building model, supervised at scale by a VLM-distilled material passport over 1.9M elements. The attributes ride the existing token space and condition on each element's own geometry through self-attention, so they cost nothing to add: the material-aware model matches the layout-only baseline on the same splits. That same design keeps the grammar extensible, since new attributes append without renumbering or decoder changes, and every command still maps one-to-one onto a native Revit object and IFC entity, which we validate end-to-end. Along the way we find that decoding these programs is bound by overhead rather than compute, and that what now limits metric precision is detection rather than the token grid. Representing a building as language brings as-built BIM ingestion within reach, and makes the reconstructed asset a direct input to LLM-driven, sustainability-aware reasoning.

References

1. Abouagour, M., Garyfallidis, E.: Resplan: A large-scale vector-graph dataset of 17,000 residential floor plans (2025), https://arxiv.org/abs/2508.14006 3
2. Abualdenien, J., Borrmann, A.: Formal analysis and validation of levels of geometry (log) in building information models (2020), https://api.semanticscholar.org/CorpusID:220493703 2
3. Armeni, I., Sax, S., Zamir, A.R., Savarese, S.: Joint 2d-3d-semantic data for indoor scene understanding (2017), https://arxiv.org/abs/1702.01105 3
4. Avetisyan, A., Khanova, T., Choy, C., Dash, D., Dai, A., Nießner, M.: SceneCAD: Predicting object alignments and layouts in RGB-D scans. In: ECCV (2020) 3

5. Avetisyan, A., Xie, C., Howard-Jenkins, H., Yang, T.Y., Aroudj, S., Patra, S., Zhang, F., Frost, D., Holland, L., Orme, C., Engel, J., Miller, E., Newcombe, R., Balntas, V.: SceneScript: Reconstructing scenes with an autoregressive structured language model. In: ECCV (2024). https://doi.org/10.1007/978-3-031-73030-6_14 2, 3, 7
6. Bell, S., Upchurch, P., Snavely, N., Bala, K.: OpenSurfaces: A richly annotated catalog of surface appearance. ACM TOG **32**(4) (2013) 4
7. Bell, S., Upchurch, P., Snavely, N., Bala, K.: Material recognition in the wild with the materials in context database. In: CVPR (2015) 4
8. Bieri, V., Rakotosaona, M.J., Tateno, K., Engelmann, F., Guibas, L.: HouseLayout3D: A Benchmark and Training-free Baseline for 3D Layout Estimation in the Wild. In: Conference on Neural Information Processing Systems (NeurIPS) (2025) 3
9. Byers, B.S., Raghu, D., Olumo, A., De Wolf, C., Haas, C.: From research to practice: A review on technologies for addressing the information gap for building material reuse in circular construction. Sustainable Production and Consumption **45**, 177–191 (2024). https://doi.org/10.1016/j.spc.2023.12.017 2
10. Cai, T., Li, Y., Geng, Z., Peng, H., Lee, J.D., Chen, D., Dao, T.: Medusa: Simple LLM inference acceleration framework with multiple decoding heads. In: ICML (2024) 4, 10
11. Chen, C., Borgeaud, S., Irving, G., Lespiau, J.B., Sifre, L., Jumper, J.: Accelerating large language model decoding with speculative sampling. arXiv preprint arXiv:2302.01318 (2023) 4
12. Choy, C., Gwak, J., Savarese, S.: 4D spatio-temporal ConvNets: Minkowski convolutional neural networks. In: CVPR (2019) 4
13. Dai, A., Chang, A.X., Savva, M., Halber, M., Funkhouser, T., Nießner, M.: ScanNet: Richly-annotated 3D reconstructions of indoor scenes. In: CVPR (2017) 3
14. De Wolf, C., Byers, B.S., Raghu, D., Gordon, M., Schwarzkopf, V., Triantafyllidis, E.: D5 digital circular workflow: five digital steps towards matchmaking for material reuse in construction. npj Materials Sustainability **2**(1), 36 (Nov 2024). https://doi.org/10.1038/s44296-024-00034-8 2
15. Deitke, M., VanderBilt, E., Herrasti, A., Weihs, L., Salvador, J., Ehsani, K., Han, W., Kolve, E., Farhadi, A., Kembhavi, A., Mottaghi, R.: ProcTHOR: Large-Scale Embodied AI Using Procedural Generation. In: NeurIPS (2022) 3
16. Engel, J., Somasundaram, K., Goesele, M., Sun, A., Gamino, A., Turner, A., et al.: Project Aria: A new tool for egocentric multi-modal AI research. arXiv preprint arXiv:2308.13561 (2023) 7
17. Ganin, Y., Bartunov, S., Li, Y., Keller, E., Saliceti, S.: Computer-aided design as language. In: NeurIPS (2021) 3
18. Ganon, K., Alper, M., Mikulinsky, R., Averbuch-Elor, H.: Waffle: Multimodal floorplan understanding in the wild (2024), https://arxiv.org/abs/2412.00955 3
19. Gemma Team: Gemma 3 technical report. arXiv preprint arXiv:2503.19786 (2025) 4, 7
20. Gloeckle, F., Youbi Idrissi, B., Rozière, B., Lopez-Paz, D., Synnaeve, G.: Better & faster large language models via multi-token prediction. In: ICML (2024) 4, 10
21. Gray, A.: Getting started with CUDA graphs. NVIDIA Developer Technical Blog, https://developer.nvidia.com/blog/cuda-graphs/, [Accessed 26-07-2026] 4
22. He, K., Zhang, X., Ren, S., Sun, J.: Deep residual learning for image recognition. In: CVPR (2016) 8

23. Heisel, F., Rau-Oberhuber, S.: Calculation and evaluation of circularity indicators for the built environment using the case studies of UMAR and Madaster. Journal of Cleaner Production **243**, 118482 (2020) 4, 14
24. Honic, M., Kovacic, I., Rechberger, H.: Improving the recycling potential of buildings through material passports (MP): An austrian case study. Journal of Cleaner Production **217**, 787–797 (2019) 4
25. International Organization for Standardization: ISO 16739-1:2018 — industry foundation classes (IFC) for data sharing in the construction and facility management industries. ISO Standard (2018) 2
26. Kuhn, H.W.: The Hungarian method for the assignment problem. Naval Research Logistics Quarterly **2**(1–2), 83–97 (1955) 11
27. Labs, P.: GitHub - pyrevitlabs/pyRevit: Rapid Application Development (RAD) Environment for Autodesk Revit® — github.com. https://github.com/pyrevitlabs/py{R}evit, [Accessed 26-07-2026] 13
28. Leviathan, Y., Kalman, M., Matias, Y.: Fast inference from transformers via speculative decoding. In: ICML (2023) 4
29. Liu, C., Wu, J., Furukawa, Y.: Floornet: A unified framework for floorplan reconstruction from 3d scans (2018), https://arxiv.org/abs/1804.00090 3
30. Liu, Y., Liu, C., Wang, B., Jiao, W., Wu, B., Fan, L., Chen, Y., Li, F., Xiong, B.: Cage: Continuity-aware edge network unlocks robust floorplan reconstruction (2025), https://arxiv.org/abs/2509.15459 3
31. Liu, Y., Zhu, L., Ma, X., Ye, H., Gao, X., Zheng, X., Shen, S.: Polyroom: Room-aware transformer for floorplan reconstruction (2024), https://arxiv.org/abs/2407.10439 3
32. Loshchilov, I., Hutter, F.: Decoupled weight decay regularization. In: ICLR (2019) 11
33. Luscuere, L.M.: Materials passports: Optimising value recovery from materials. Proceedings of the Institution of Civil Engineers — Waste and Resource Management **170**(1), 25–28 (2017) 4, 14
34. Macher, H., Landes, T., Grussenmeyer, P.: From point clouds to building information models: 3D semi-automatic reconstruction of indoors of existing buildings. Applied Sciences **7**(10), 1030 (2017) 2, 3
35. Naikade, P., Frederik, L., Jensen, M.B., Elmholdt, K.T., Møgelmose, A.: Xrai for intelligent and sustainable aec: Survey on integrating extended reality and artificial intelligence for human-centric built environments (May 2026). https://doi.org/10.5281/zenodo.20283895 4
36. Nash, C., Ganin, Y., Eslami, S.M.A., Battaglia, P.W.: PolyGen: An autoregressive generative model of 3D meshes. In: ICML (2020) 3
37. OpenAI: GPT-4 technical report. arXiv preprint arXiv:2303.08774 (2023) 14
38. Oquab, M., Darcet, T., Moutakanni, T., Vo, H., Szafraniec, M., Khalidov, V., et al.: DINOv2: Learning robust visual features without supervision. TMLR (2024) 8
39. Panagoulia, E., Rakha, T.: Data reliability in bim and performance analytics: A survey of contemporary aeco practice. Journal of Architectural Engineering **29**(2), 04023006 (2023). https://doi.org/10.1061/JAEIED.AEENG-1483 2
40. Pomponi, F., Moncaster, A.: Circular economy for the built environment: A research framework. Journal of Cleaner Production **143**, 710–718 (2017) 4, 14
41. Programme, U.N.E.: Building materials and the climate: Constructing a new future. https://wedocs.unep.org/handle/20.500.11822/43293 (2023), [Accessed 12-12-2025] 2
42. Schwartz, G., Nishino, K.: Recognizing material properties from images. IEEE TPAMI **42**(8), 1981–1995 (2020) 4

43. Shazeer, N.: Fast transformer decoding: One write-head is all you need. arXiv preprint arXiv:1911.02150 (2019) 4
44. Siméoni, O., Vo, H.V., Seitzer, M., Baldassarre, F., Oquab, M., Jose, C., et al.: DINOv3. arXiv preprint arXiv:2508.10104 (2025) 8
45. Soust-Verdaguer, B., Llatas, C., García-Martínez, A.: Critical review of BIM-based LCA method to buildings. Energy and Buildings **136**, 110–120 (2017) 4, 14
46. Stekovic, S., Rad, M., Fraundorfer, F., Lepetit, V.: Montefloor: Extending mcts for reconstructing accurate large-scale floor plans (2021), https://arxiv.org/abs/2103.11161 3
47. Stern, M., Shazeer, N., Uszkoreit, J.: Blockwise parallel decoding for deep autoregressive models. In: NeurIPS (2018) 4
48. Tang, H., Liu, Z., Li, X., Lin, Y., Han, S.: TorchSparse: Efficient point cloud inference engine. In: Machine Learning and Systems (MLSys) (2022) 4, 20
49. Tang, P., Huber, D., Akinci, B., Lipman, R., Lytle, A.: Automatic reconstruction of as-built building information models from laser-scanned point clouds: A review of related techniques. Automation in Construction **19**(7), 829–843 (2010) 2, 3
50. UN-Habitat: Future cities advisory outlook 2023: Digital innovations empower urban net-zero carbon transition. https://unhabitat.org/future-cities-advisory-outlook-2023 (2023), [Accessed 12-11-2025] 2
51. Upchurch, P., Niu, R.: A dense material segmentation dataset for indoor and outdoor scene parsing. In: ECCV (2022) 4
52. U.S. Institute of Building Documentation: USIBD level of accuracy (LOA) specification guide, version 3.0. Specification C220-2019 (2019) 2, 10
53. Vaswani, A., Shazeer, N., Parmar, N., Uszkoreit, J., Jones, L., Gomez, A.N., Kaiser, L., Polosukhin, I.: Attention is all you need. In: NeurIPS (2017) 3
54. Volk, R., Stengel, J., Schultmann, F.: Building information modeling (BIM) for existing buildings — literature review and future needs. Automation in Construction **38**, 109–127 (2014) 2, 3
55. Wu, R., Xiao, C., Zheng, C.: DeepCAD: A deep generative network for computer-aided design models. In: ICCV (2021) 3
56. Xie, C., Avetisyan, A., Howard-Jenkins, H., Siddiqui, Y., Straub, J., Newcombe, R., Balntas, V., Engel, J.: Human-in-the-loop local corrections of 3d scene layouts via infilling. arXiv preprint arXiv:2503.11806 (2025) 3, 10
57. Xu, H., Xu, J., Huang, Z., Xu, P., Huang, H., Hu, R.: Fri-net: Floorplan reconstruction via room-wise implicit representation (2024), https://arxiv.org/abs/2407.10687 3
58. Yin, R., Shi, X., Bailo, O., Manfredi, M., Gevers, T.: Fast SceneScript: Fast and accurate language-based 3D scene understanding via multi-token prediction. arXiv preprint arXiv:2512.05597 (2025) 3
59. Yue, Y., Kontogianni, T., Schindler, K., Engelmann, F.: Connecting the dots: Floorplan reconstruction using two-level queries (2023), https://arxiv.org/abs/2211.15658 3
60. Zheng, J., Zhang, J., Li, J., Tang, R., Gao, S., Zhou, Z.: Structured3d: A large photo-realistic dataset for structured 3d modeling (2020), https://arxiv.org/abs/1908.00222 3

Supplementary Material

A Material Language and Passport Details

Extraction. Figure 6 shows the material and condition extraction pipeline on one scene. The label written into the language is the VLM's; the dense-segmentation and classical-CV cues are computed and retained in the passport as an independent check rather than merged into it (Tab. 6). Labels are canonicalized by stripping parenthetical suffixes and mapping to atomic `snake_case`. The confidence floor is 0.7: anything that fails the join to a ground-truth element, is never observed, falls below that floor, or carries an out-of-vocabulary label becomes an explicit `unknown` rather than a guessed or a dropped label, and every such case is counted. Composite component break-downs are kept in the passport JSON and never enter the language.

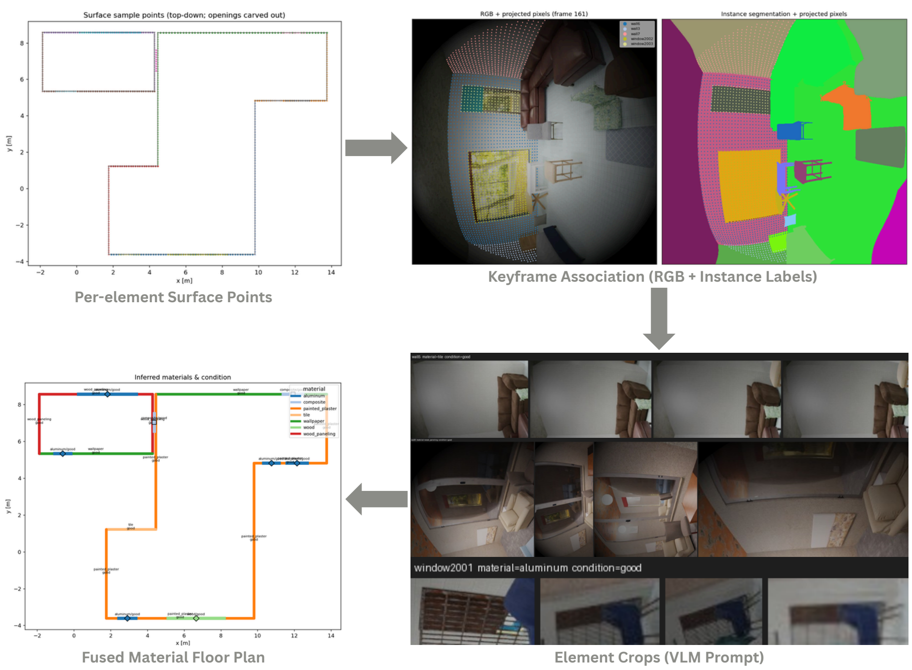

Fig. 6: Material-passport extraction on one scene. Surface points are associated to elements, the observing keyframes are projected onto each element to cut per-element crops, and the fused per-element label is written back as a material- and condition-annotated floor plan. The crops are what the vision-language model actually sees, which is why occlusion filtering (Sec. 4.3) matters: an unfiltered crop can show the wrong surface entirely.

Table 6: The BIMScript dataset and material-passport corpus extracted from ASE dataset. Cross-cue agreement indicates label uncertainty (Sec. 4.2).

Corpus		*Materials*		*Conditions*	
Scenes (total)	99,990	aluminum	20.5%	good	83.0%
skipped/missing	10	wallpaper	19.1%	new	12.9%
train split	97,990	painted_plaster	14.0%	worn	3.7%
val split	1,000	wood_paneling	13.1%	damaged	0.05%
test split	1,000	wood	10.3%	unknown	0.4%
Elements	1,900,908	composite	9.1%		
Join failures	0	tile	6.3%		
Material classes	14	concrete	2.5%		
Condition classes	5	stone	1.7%		
		metal	1.4%		
		brick	1.2%		
Cross-cue agreement		pvc	0.3%		
VLM vs. classical CV	∼25%	glass	0.04%		
VLM vs. dense seg.	∼34%	unknown	0.4%		

B Implementation and Decoding Details

CUDA-graph. CUDA-graph decoding uses per-context-length buckets and recaptures only when a scene's context exceeds the current bucket. The FSM device tables encode the parameter-to-next-parameter progression and the command-to-first-parameter mapping; the `PART` and `STOP` helper tokens override that progression from the sampled value itself, applied branchlessly so the graph never needs a host synchronization to decide a type.

Intra-element redrafting. One-shot drafts accept only 38% of slots, because coupled coordinates such as a wall's far corner given its near corner are genuinely ambiguous before any value is fixed. Two measures recover much of this. First, the infill objective masks *whole elements*, matching draft-time conditioning exactly. Second, after a rejection the remaining slots are redrafted with all accepted values as real context, two forwards per round, so each round converts resolved ambiguity into acceptances and the worst case degrades gracefully toward sequential decoding. Redrafting lifts acceptance to 51%. Doubling the fine-tune budget changes nothing (50.8% vs 51.0%), which is what indicates the residual gap is coordinate-coupling ambiguity rather than undertraining. Folding the draft and verify passes into GraphStep's graph, and a strict τ=0 variant that would recover output-exactness, are future work.

fp16 encoder. We tried inference-time fp16 autocast on the sparse encoder and measured essentially no gain: the TorchSparse [48] library's custom kernels carry no autocast rules and silently stay fp32, so only the encoder's few dense layers cast. A genuine encoder speed-up needs true fp16 through the sparse kernels, so we deprioritized it.

Sub-bin refinement. Table 7 reports per-type coordinate MAE and mean F1 at tight thresholds, conditional on an already-correct detection: shared, matched elements only. We do not report an end-to-end precision number over all ground-truth entities, which would additionally penalize missed and spurious detections.

Table 7: Sub-bin refinement, conditional on correct detection (64 scenes, shared detections, matched elements). Per-type coordinate MAE (cm) and mean F1 at tight thresholds.

	MAE (cm) ↓			mean F1 ↑	
Method	wall	door	window	F1@1cm	F1@2cm
no refinement (5cm grid)	8.74	1.74	2.77	0.001	0.034
+ geometric snapping	8.37	1.74	2.75	0.001	0.034
+ SubBin offset head	8.61	**1.56**	**2.68**	**0.004**	**0.071**

C SceneScript Reproduction Audit Details

Discretization and reconstruction. The unbiased pairing are floor with center or round-at-discretize with edge reconstruction; either gives per-axis quantization error in $[-2.5, +2.5)$ cm, and $[-2, +2)$ cm for height, so a purely arithmetic, model-free round-trip has worst-case per-corner error $\sqrt{2.5^2 + 2.5^2 + 2^2} = 4.06$ cm. A controlled A/B on the public checkpoint (100 validation scenes) identifies which convention is consistent with the released weights: edge reconstruction scores 0.570 F1@5cm while center reconstruction collapses to 0.154. This identifies a convention consistent with the weights; it is not a direct observation of SceneScript's training recipe.

Translation-frame removals. The frame's origin is the lowest observed point in the point cloud, so anything the scan did not cover falls at a negative coordinate, outside the range the tokenizer can represent. Ground truth, though, describes the whole floor plan: a room the camera never entered still has walls in it, and those are exactly the ones that land out of range. The tokenizer drops them silently, so the model is trained never to predict them. The cost is therefore a quiet loss of recall rather than a visible error, which is why it went unnoticed until we logged it. Over one live training run this happened 46,218 times across 14,395 scene-visits, at least 14.5% of the scenes seen, and 92% of what disappeared were walls. Because a run revisits every scene once per epoch, these are removal *events* rather than unique elements; the same wall in the same scene is counted again each time it comes round. Anchoring the frame at the point-cloud minimum *minus* a margin, with a bounded clamp for small overshoots, brings the residual cost down to 0.6% of entities at evaluation time.

Round-trip diagnostic. This measures the ceiling that the tokenizer imposes on any model. It normalizes, discretizes, and reconstructs the ground truth with the same functions used at train and eval time, then scores the result against the un-round-tripped ground truth (300 validation scenes, 5,546 entities, rotation disabled so quantization is the only error source). A model that predicted every bin correctly would score exactly this and no higher. The world frame spans 32 m, so one bin is 5 cm at 640 and 1.56 cm at 2,048, and round-to-nearest leaves at most half a bin of per-axis error. At 640 bins the round trip scores 0.994 mean F1@5cm (per-class 0.987 wall, 0.999 door, 0.995 window). The shortfall from 1.0 is not rounding, which at ± 2.5 cm per axis stays well inside the 5 cm threshold, but the 0.6% of entities dropped as out of frame: $1 - 0.006 = 0.994$ recovers the

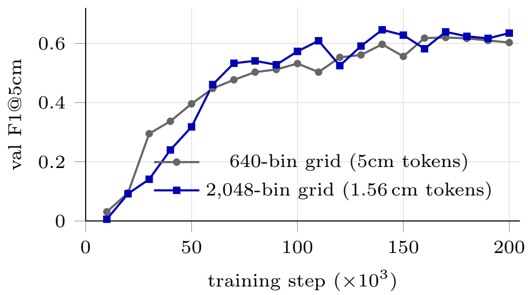

Fig. 7: Validation F1@5cm over training for the two language grids (in-run 64-scene slice, identical data, recipe, and step count). The 3.2× finer grid starts slower, since each coordinate needs more optimization, and then overtakes once the model's residual token error shrinks to a few bins, which is exactly where grid pitch decides whether that error passes or fails the 5cm test. The two curves end within the slice's own eval-to-eval noise, consistent with the small margin in Tab. 1.

measured value. AvgF1 behaves differently because it averages F1 over thresholds well below one bin width, where quantization does bind: the ceiling is 0.845 at 640 bins and 0.970 at 2,048. That difference is the headroom the finer grid opens, and the reason its benefit appears at strict thresholds rather than coarse ones. This is a diagnostic rather than a replication of the training-time pipeline, which additionally applies rotation augmentation and wall/opening host reassignment.

Anchor stability. The frame origin is the point-cloud minimum less the margin, and the cloud is capped at 500k points, so for large scenes the origin depends on which points survive subsampling. On the same 300 scenes, 60 (20%) exceed the cap; across three random draws each, the origin moves by a median of 0.41 m in L_∞, a 90th percentile of 1.41 m, and at most 2.00 m, with 45 of the 60 moving more than 5 cm. The 90th percentile alone exceeds the 1.0 m margin. Cloud and language are translated together, so each sample stays internally consistent and the effect acts as additional translation jitter during training; at evaluation it makes the frame, and hence which entities are clamped or dropped, depend on the draw. The round-trip diagnostic above anchors on the full-cloud minimum, so the 0.6% residual is measured under a stable anchor and is a lower bound on what the live pipeline sees.

Schedule sensitivity. We trained two from-scratch probes at vocabulary 2,048 on the full corpus. Our recipe (LR 10^{-4}, cosine, 100k steps) stays healthy across classes (window F1@5cm 0.386); the Fast SceneScript recipe (LR 10^{-3}, multi-step decay, 92k steps) converges walls and doors (0.563/0.778) but collapses windows to 0.058 and never recovers. The aggressive schedule locks into a wall/door-optimal basin before windows, the most evidence-sparse class, can catch up. We default to cosine.

Convergence budget. At an equal 100k budget the finer grid trails at 5cm, since a 3.2× finer vocabulary needs more optimization per coordinate. Table 1 therefore uses a matched 200k budget, where it leads on strict F1 and trails on the coarse average; Fig. 7 traces validation F1@5cm for both grids under identical data, recipe, and step count.

D BIMScript-to-BIM Mapping and Additional Results

Figure 8 shows uncurated ground-truth/prediction pairs with corner insets for the first three validation scenes. Two failure modes dominate what the strict-F1 numbers measure. Walls bounding *unexplored* floor area are unsupported by points and are either missed or placed with large error, and coordinate error concentrates in z, where the range is narrower than in x/y so the same bin error is a larger fraction of the extent. Figure 9 renders decoded programs in 3D with their predicted materials.

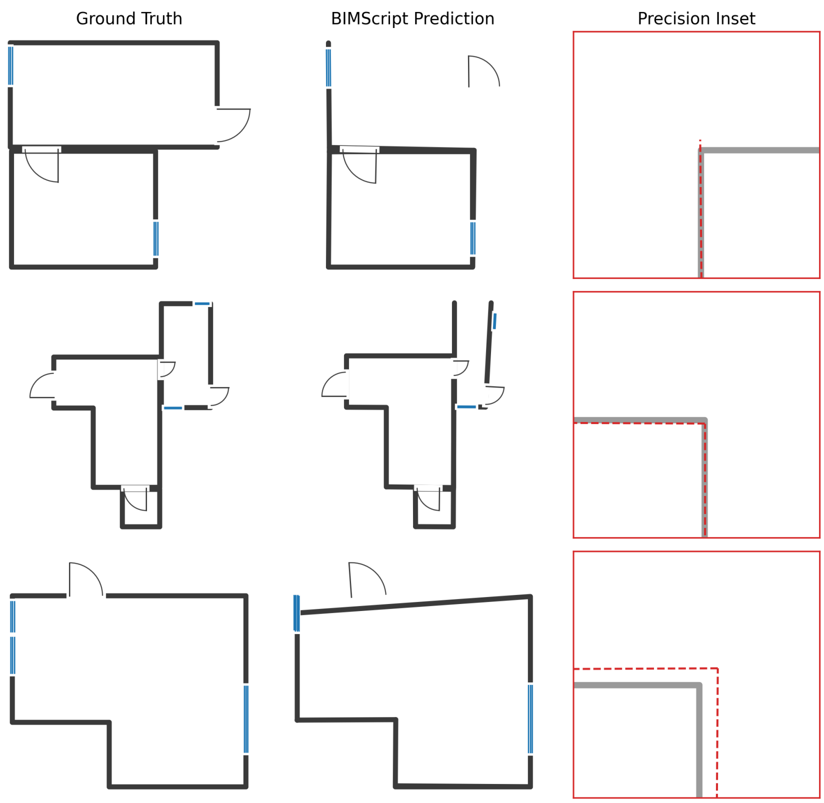

Fig. 8: Qualitative layout results on the first three validation scenes: ground truth, BIMScript prediction, and a zoomed corner inset (GT solid, prediction dashed); doors are drawn as swing arcs, windows as blue sill glyphs. Rows 1–2 show typical centimeter-level corner agreement; row 3 shows a residual corner offset, and row 1 a missed wall segment, the failure modes behind the strict-F1 numbers in Tab. 1.

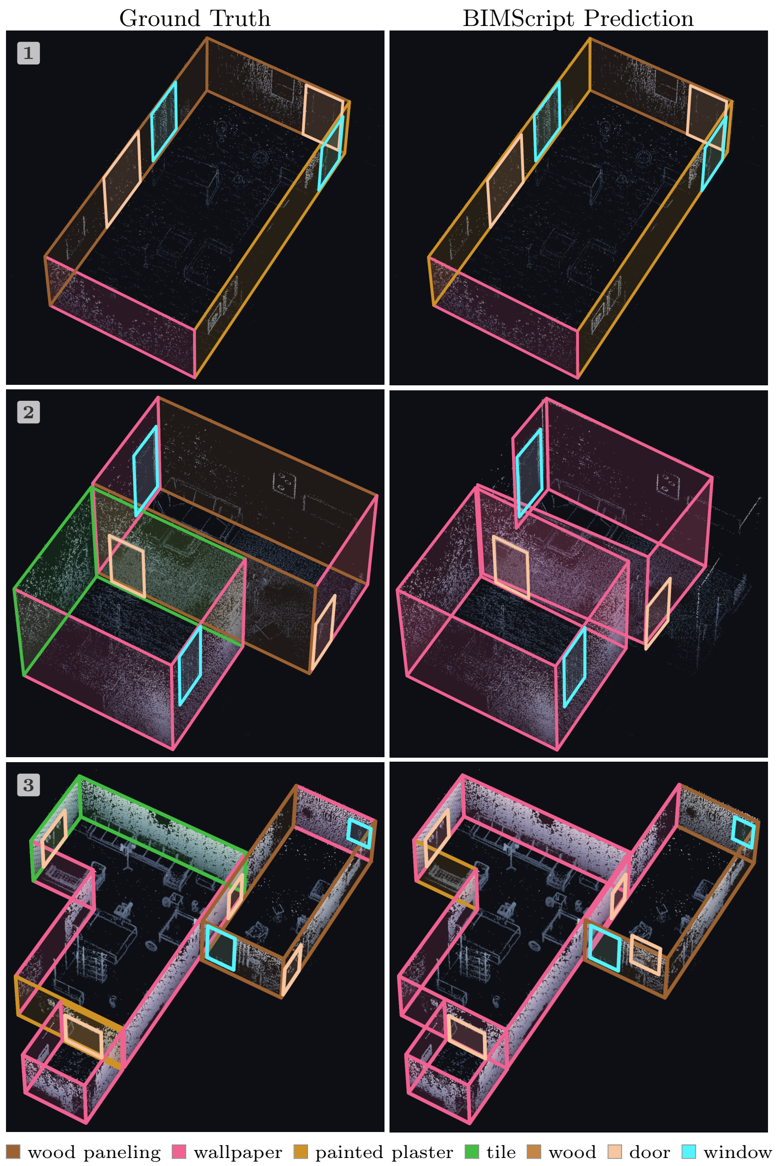

Fig. 9: Decoded programs rendered in 3D over the input point cloud. Geometry tracks the ground truth closely, and openings are placed on the correct host walls. The materials show both regimes behind the numbers in Tabs. 3 and 4: scene 1 recovers exactly the five materials present in its ground truth, whereas scene 2 collapses tile and wood paneling into the corpus-frequent `wallpaper`, which is what a material accuracy of 0.63 alongside a macro-F1 of 0.29 looks like element by element. Door and window materials (`composite`, `aluminum`) are recovered essentially always, since they are near-deterministic given the element class.